Published in final edited form as:

IEEE Trans Med Imaging. 2017 May ; 36(5): 1129–1139. doi:10.1109/TMI.2017.2652502.

A Method for Measuring Orientation within a Magnetic Resonance Imaging Scanner using Gravity and the Static Magnetic Field (VectOrient)

Adam van Niekerk,

Department of Human Biology, Biomedical Engineering, University of Cape Town, South Africa

Andre van der Kouwe [Senior Member, IEEE], and

Athinoula A. Martinos Center, Massachusetts General Hospital, Charlestown, MA, United States and Radiology, Harvard Medical School, Boston, MA, United States

Ernesta Meintjes

Department of Human Biology, Biomedical Engineering, University of Cape Town, South Africa

Abstract

In MRI brain imaging, subject motion limits obtainable image clarity. Due to the hardware layout of an MRI scanner, gradient excitations can be used to rapidly detect position. Orientation, however, is more difficult to detect and is commonly calculated by comparing the position measurements of multiple spatially constrained points to a reference dataset. The result is increased size of the apparatus the subject must wear, which can influence the imaging workflow. In optical based methods marker attachment sites are limited due to the line of sight requirement between the camera and marker, and an external reference frame is introduced. To address these challenges a method called VectOrient is proposed for orientation measurement that is based on vector observations of gravity and the MRI scanner's static magnetic field. A prototype device comprising of an accelerometer, magnetometer and angular rate sensor shows good MRI compatibility. Phantom scans of a pineapple with zero scanner specific calibration achieve comparable results to a rigid body registration algorithm with deviations less than 0.8 degrees over 28 degree changes in orientation. Dynamic performance shows potential for prospective motion correction as rapid changes in orientation (peak 20 degrees per second) can be corrected. The pulse sequence implemented achieves orientation updates with a latency estimated to be less than 12.7 ms, of which only a small fraction (<1 ms) is used for computing orientation from the raw sensor signals. The device is capable of quantifying subject respiration and heart rates. The proposed approach for orientation estimation could help address some limitations of existing methods such as orientation measurement range, temporal resolution, ease of use and marker placement.

Index Terms

Orientation; Accelerometer; Magnetometer; MRI; Angular Rate; Prospective Motion Correction

I. Introduction

MAgnetic resonance imaging (MRI) is vulnerable to subject motion due to the time required to acquire the data needed for image reconstruction. The signal is spatially encoded by manipulating the magnitude of the magnetic field in three orthogonal directions at different times during the signal acquisition. Typically, the acquisition needs to be repeated for many different magnetic field gradients as the physical space within the scanner is encoded in the spatial frequency domain (k-space). Any motion that occurs during image acquisition results in the signal being mapped to incorrect locations causing ghosting and blurring and manifest as artefacts in the resulting images. To further complicate the problem, the magnetic susceptibility of the imaged region usually varies over 'material' boundaries such as tissue-air (sinuses), and tissue-cerebral spinal fluid (ventricles). As a result motion affects the homogeneity of the main magnetic field, because shimming to correct for these susceptibility changes is pose specific.

Advances in acquisition technologies now allow for submillimetre spatial encoding of the physical space within the MRI scanner in only a few minutes. Due to an increase in required imaging resolution minute motion and physiological movements (such as the cardiac and respiration cycles) play a limiting role in obtainable image clarity even for healthy subjects who move very little [1]. Subject motion has therefore become a critical aspect in high resolution imaging and remains one of the biggest challenges in difficult to scan populations such as the old and very young where sedation is generally impractical, expensive and in the case of research not admissible due to ethical reasons.

Physically, the spatial encoding of the magnetic field within the MRI scanner is fixed with respect to translation, having a point of zero effect known as the gradient iso-centre. Any combination of the x, y and z gradients is therefore physically constrained to a rotation about this single point. Translations in image space are implemented by imposing phase rolls across the corresponding direction in the k-space representation of the measured signal. Therefore identical gradient waveforms (except gradients which select a region in space if slice-selective, but don't play a role in spatial encoding) will be used to image identical field of views (FOVs) at two different locations (same orientation) in the MRI scanner. If an object changes orientation within an MRI scanner and one applies an incorrectly oriented version of the pulse sequence, magnetisation will be different and contrast will be affected as the relative magnitude of the magnetic field at each point on the object has changed. Translation is a macro effect that introduces a bias in the frequency of the net signal received from the imaged object proportional to the applied gradient vector. Each time a gradient waveform is played out a constant frequency offset needs to be interpreted correctly to ensure correct image encoding. Any error in translation between the measurement frame and the pulse sequence frame will manifest in a phase roll as each point is sampled in the incorrect reference frame. Incorrect interpretation of how the signal is received doesn't affect how the spins were spatially de/re-phased relative to each other to form the image and therefore won't effect the magnitude of the MR signal (in an idealised MRI scanner).

Retrospective motion correction techniques rely on correcting/adjusting k-space after the data has been collected. Besides effects caused by discretely sampling the signal such as

aliasing, the effects of translation can be corrected retrospectively if it is known (and the correct spins were excited). Retrospective correction of orientation, even if the motion was tracked perfectly, would still have errors due to spin history effects and an inconsistently sampled version of k-space. Rapid correction of orientation is therefore paramount to ensuring stability of the magnitude of the raw MR signal as the physical formation of the image is directly related to orientation; rotating k-space rotates the image by the same angle. This has led to the development of prospective motion correction in which motion parameters are tracked and corrections are applied to the pulse sequence as frequently as possible during the image acquisition. Prospective motion correction is realised by altering the way in which the linear combination of the x,y and z gradients contribute to the predefined waveforms (orientation) of the pulse sequence and the relative frequency at which the raw MR signal is demodulated (translation) to effectively follow a rigid object as it moves within the MRI scanner. In the case of neuro-imaging the brain is modeled as rigid, even though small amplitude (50μm) plastic deformation is present [2].

A. Measuring Orientation using Gradient Encoding

In most cases orientation is measured using the gradient coil system of the MRI scanner. These techniques inherit the co-ordinate frame of the imaging sequence allowing them to be calibration free. Intuitively one can use the same principles used for image acquisition to track orientation in the image domain. Low resolution 3D image acquisitions [3] (vNav) or a series of 3 orthogonal 2D spiral acquisitions [4] (PROMO) are inserted into the existing pulse sequence. These approaches then co-register subsequent lower resolution images to an initial reference image to measure the change in subject pose. The information rich dataset can also be used to correct for changes in the homogeneity of the scanner's magnetic field. These methods do, however, have limited temporal resolution and can fail during rapid motion or completely miss small periodic motion. Fast k-space navigators [5] overcome some of the temporal resolution limitations of these techniques, at the cost, however, of increased sequence dependence or the need for reference datasets that can affect the accuracy of motion measurements. Free induction decay navigators [6] form a useful tool for detecting motion, however they don't have sufficient information for pulse sequence correction.

External hardware can be introduced to improve the robustness of orientation estimates of k-space navigator approaches, such as active markers [7] or inductive coils [8]. These approaches overcome some of the challenges of measuring orientation in the frequency domain (k-space) by physically encoding orientation using translation measurements of multiple points. A linear combination of gradients can only encode position in one direction at any instant in time. Three different (preferably orthogonal) gradient pulses can be inserted into the pulse sequence to measure the position of one or multiple points in the gradient co-ordinate frame. To fully constrain the orientation a minimum of 3 points (active markers) or 2 points and the direction of the gradient flux vector (inductive coils) are required to uniquely define the orientation of the tracked object. The requirement for 3 unique gradient excitations that wouldn't normally be present in the imaging pulse sequence means that motion measurement is restricted as new excitations could affect the quality of the resulting image. This is especially true in Echo Planar Imaging (EPI) sequences where long

uninterrupted echo trains are required. Gradient tones [9] allow a reduction in pulse sequence impact, however this comes at the cost of reduced achievable slew rate and still requires multiple markers.

B. Sequence Independent Approaches

Sequence independent methods measure motion parameters using external hardware, such as optical motion tracking [10]. Independence of the pulse sequence allows for versatile and rapid acquisition of motion parameters. The use of a camera to track an in-bore marker which has a limited measurement range does however introduce new challenges such as camera mounting, MR compatibility, marker line-of-sight, lighting and the introduction of a new reference frame that has to be calibrated to a fixed camera position making it time consuming to set up [11].

C. Challenges in Orientation Measurement

The pulse sequence modifications required for gradient based methods and increased complexity of current sequence independent techniques have resulted in prospective motion correction using external hardware having a limited impact in clinical MRI even though it has been proven to be effective. In most current external motion tracking techniques orientation isn't measured directly. Rapid translation measurements of multiple points are used to encode orientation ([7], [10], [8], [12]). The distance between each of the points must be kept constant throughout the image acquisition for comparison to the initial positions to remain valid. To achieve the same precision for orientation as translation measurements these points should enclose the entire imaging volume, making the apparatus the subject has to wear large. To address this challenge specialised retrogate markers have been implemented which spatially encode orientation on the marker itself using *Moire patterns* ([13]). In this method there is still however a tradeoff between size and precision and restriction of line of sight makes the marker more vulnerable to motion relative to the subject.

D. VectOrient - An alternative approach

An orientation measurement technique requiring just a single marker would complement existing methods, and could, if combined with a single translation measurement, allow for rigid body motion correction from a single point. Knowledge of orientation greatly reduces the challenges associated with k-space navigator design and could benefit self-navigated pulse sequences or complement retrospective techniques. We demonstrate here a vector based approach to orientation measurement that does not require spatially encoding orientation. The device relies on measuring the direction of the static magnetic field and gravity. The magnetic field vector and gravity are both observable from any point within the scanner bore which allows one to mount the marker anywhere on the 'rigid' body of interest, in any orientation, because there are no restrictions on measurement range or line-of-sight. The vectors are also both well defined relative to the scanner gradient co-ordinate system. The proposed orientation tracking method is therefore calibration free, to the extent that the scanner's construction is accurate, whilst remaining sequence independent.

II. Theory

The MRI environment is unique in that there exists a static magnetic field that is exceptionally stable over time. A small Hall effect magnetometer can be used to measure this vector very precisely due to the large magnitude of the physical field. A single vector observation, in this case the scanner's static magnetic field, constrains the sensor's orientation relative to any frame in which that vector is known to a single degree of freedom about the axis of the observed vector. To fully define the sensor's orientation relative to the reference frame another measurement that is not parallel/anti-parallel to the existing observation is required. During an MRI scan, the patient spends the majority of the time at rest. During these periods the accelerometer gives an estimate of the direction of gravity in the sensor frame. It is important to note that the accelerometer measures the resultant of the forces acting on a proof mass and not the total acceleration:

$$\vec{a} = \frac{\vec{F}_{\text{body}} - m_{\text{proof}}\vec{g}}{m_{\text{proof}}}$$

Therefore, during periods when the patient is still ($F_{body} = 0$), the accelerometer measures:

$$\vec{a} = -\vec{g}$$

Even though the sensor itself is in equilibrium and not accelerating. This fully constrains the sensor's orientation in a reference frame where both the directions of $\vec{B}_0$ and $\vec{g}$ are known, in fact the problem is now over-constrained.

Fig. 1 describes a conventional MRI scanner layout in which gravity ($\vec{g}$), which lies normal to the patient bed, and the static magnetic field ($\vec{B}_0$), which runs axially along the scanner bore, are almost perfectly orthogonal to each other. As part of the main magnet installation as specified by the 3 T Skyra (Siemens, Erlangen, Germany) used in this work, pendulums are used for aligning the scanner YZ plane to gravity.

This justifies two assumptions made for the scanner reference frame:

- Gravity lies on the YZ plane of the gradient fields.
- The static magnetic field and the gradient Z-axis are parallel, misalignment would cause gradient torques increasing the scanner noise.

A. From Vector Observations to Orientation

Based on the assumptions made one can define the following reference matrix **H** without any calibration between the sensor and scanner frames:

$$\overline{\mathbf{h}}_1 = \frac{\vec{B}_0 \times \vec{g}}{\|\vec{B}_0 \times \vec{g}\|}$$

$$\overline{\mathbf{h}}_{\mathbf{2}}=\frac{\overrightarrow{B}_0\times\overline{\mathbf{h}}_{\mathbf{1}}}{\|\overrightarrow{B}_0\times\overline{\mathbf{h}}_{\mathbf{1}}\|}$$

$$\overline{\mathbf{h}}_{\mathbf{3}}=\frac{\overrightarrow{B}_0}{\|\overrightarrow{B}_0\|}$$

$$\mathbf{H}=\begin{pmatrix}\overline{\mathbf{h}}_{\mathbf{1}}\\ \overline{\mathbf{h}}_{\mathbf{2}}\\ \overline{\mathbf{h}}_{\mathbf{3}}\end{pmatrix}=\begin{pmatrix}1&0&0\\0&1&0\\0&0&1\end{pmatrix}$$

One can then form a matrix M from the data obtained from the accelerometer $\overrightarrow{a}$ and magnetometer $\overrightarrow{m}$ which are observations of $\overrightarrow{B}_0$ and $\overrightarrow{g}$ in the sensor frame:

$$\overline{\mathbf{m}}_{\mathbf{1}}=\frac{\overrightarrow{m}\times-\overrightarrow{a}}{\|\overrightarrow{m}\times-\overrightarrow{a}\|}$$

$$\overline{\mathbf{m}}_{\mathbf{2}}=\frac{\overrightarrow{m}\times\overline{\mathbf{m}}_{\mathbf{1}}}{\|\overrightarrow{m}\times\overline{\mathbf{m}}_{\mathbf{1}}\|}$$

$$\overline{\mathbf{m}}_{\mathbf{3}}=\frac{\overrightarrow{m}}{\|\overrightarrow{m}\|}$$

$$\mathrm{M}=\begin{pmatrix}\overline{\mathbf{m}}_{\mathbf{1}}\\ \overline{\mathbf{m}}_{\mathbf{2}}\\ \overline{\mathbf{m}}_{\mathbf{3}}\end{pmatrix}$$

It follows that in this special case the rotation matrix representing the rotation from the scanner frame to the sensor frame is identical to the matrix formed by the observed normalised vectors:

$$\mathrm{M}=\mathbf{RH}=\mathbf{RI}=\mathbf{R}\quad(1)$$

The result shows that vector observations can be used to form an orthonormal rotation matrix representing the orientation of the device in the scanner frame with very few computations. It also intuitively shows the importance of the orthogonality of the vectors. As

the vectors lie more parallel to each other, the effect of noise on the unit vectors increases. During periods of motion, measurements of the direction of gravity using the accelerometer become unreliable due to accelerations of the sensor frame. These external accelerations are dealt with through a combined approach of constraining and filtering. The acceleration estimates are constrained as described above; notice that $\overline{\mathbf{m}}_2$ is formed using the vector cross product rather than just selecting gravity as the negative Y-axis. The accelerometer measurement now only affects the orientation about the axis of the static magnetic field. The acceleration measurements are then filtered such that the response to an acceleration input is of the order of 10–20 seconds. This is achieved by implementing a complementary filter that combines angular rate, magnetometer and acceleration measurements.

B. Sensor fusion

A *Mahony* [14] non-linear complementary filter (Fig. 2) was selected to fuse the sensor measurements. The observer proposed assumes an angular rate sensor model as follows:

$$\mathbf{\Omega}_a(t)=\mathbf{\Omega}_r(t)+\mu_\omega(t)+\omega_0 \quad (2)$$

Where $\mathbf{\Omega}_a(t)$ is the measured angular rate and $\mathbf{\Omega}_r(t)$ is the real/corrected angular rate, which is integrated to give the orientation estimate. The integral feedback of the filter is expected to track the slow drift in gyro bias $(\omega_0^{'} \approx \omega_0)$ and the proportional feedback compensates for noise and gyro imperfections $(\mu_\omega^{'}(t) \approx \mu_\omega(t))$. Quaternion representation of orientation was selected to allow for a more efficient execution of the algorithm on an embedded device.

C. Constraining the gravity error term

Madgwick [15] initially proposed a compensation technique to reduce the observer's sensitivity to magnetic field inhomogeneities in the application of motion tracking in rehabilitation. Apparent fluctuations in the earth's magnetic field, caused by nearby ferrous materials, cause drifts in the magnetic field vector which could affect the attitude of the output estimate. The error term generated by the magnetometer was therefore constrained to only affect the heading estimate. In the modified version proposed (Fig. 2, *Compensation block*), acceleration parallel to the observed $\overrightarrow{B}_0$ field and any slight non-orthogonality between gravity and the static magnetic field are accounted for, this allows for the assumption of gravity lying on the **YZ** plane instead of a more restricted constraint of gravity having to be parallel to the gradient **Y**-axis (see Fig. 1). The formation of the reference acceleration vector $(\overrightarrow{a}_r)$ has the same effect as the cross product $(\overline{\mathbf{m}}_2)$ in the formation of **R** in Eqn 1. By enforcing the unit constraint on the result one can efficiently calculate the compensated acceleration reference $\overrightarrow{a}_r$ because only the z-component of the rotated vector is required $(\sqrt{x^2+y^2}=\sqrt{1^2-z^2})$.

Using quaternion algebra:

$$a_r^z = \overline{a}^x (2q^x q^z - 2q^w q^y) + \overline{a}^y (2q^y q^z + 2q^w q^x) + \overline{a}^z (1 - 2q^x q^x - 2q^y q^y) \quad (3)$$

Where: $q^{w,x,y,z}$ are the elements (w scalar and x, y, z vector) of the unit quaternion representing the current estimate of the orientation. $\bar{a}^{x,y,z}$ is the acceleration measured in the sensor frame. a_r^z is the z component of the new reference vector that ensures the error term is parallel to the $\overrightarrow{B}_0$ field.

D. Filter gain selection

The implementation of the proposed observer is unique in MRI in that there exists an exceptionally stable observation of the magnetic field. Referring to Fig. 2 we select $k_1 \gg k_2$. The purpose of the gyro is mainly to improve the orientation estimates about the MRI scanner's Z-axis, during periods of motion when $\overline{a} \neq \overline{g}$. The purpose of tracking the gyro imperfections using the magnetometer is that as the orientation of the sensor frame rotates the Z-axis errors project onto the axes on the orthogonal plane. This effect was reported by [14] where a single vector observation of gravity was used to track gyro bias about the heading axis. In the present work the magnetometer complements the acceleration measurements to achieve better performance about the $\overrightarrow{B}_0$ field (Z-axis). The gains k_{1-2} are selected to be high enough such that the vector observations are weighted as highly as possible without increasing the uncertainty in the output over each time step. As a starting point the gain is selected to ensure convergence of the output and the field vector estimate at a maximum rate:

$$k_{1-2} < \frac{\tau_\omega^2}{\sigma_\theta^2} \times \mathrm{t_s} \quad (4)$$

Where: $\sigma_\theta^2(\mathrm{rad}^2)$ is the variance in the direction of the unit vector observations. $\tau_\omega(\frac{\mathrm{rad}}{\sqrt{\mathrm{s}}})$ is the gradient of the Allan deviation curve corresponding to the angular random walk (ARW) of the angular rate gyro. $\mathrm{t_s}$ is the filter iteration period.

The noise on the magnetometer σ_θ^2 is estimated as being zero mean and axis symmetric [16] and is calculated over a finite period. A similar process is followed for the selection of the accelerometer feedback gain. The data used for the variance calculation is taken from within an MRI scanner while it is active and the sensor is left motionless. It therefore includes the vibrations caused by eddy current interactions which are not considered subject motion.

The integral and proportional gains (K_i, K_p) are chosen to add up to 1 where the ratio controls the response of the filter. To prevent integral windup the rate gyro biases and initial orientation are estimated at the system start. This requires the device to be held still from 2 until 4 seconds after power up. The initial orientation is estimated from Eqn. 1 and the biases

are computed as a running average over the initialisation period. This step can be skipped and the filter will converge, albeit much slower about the axis of the static magnetic field (20 s with typical gain settings [k_2 = 1.5]).

E. Sensor Models

In reality the vector observations obtained from the sensors are not ideal, distorting the measurements from a spherical surface onto an ellipsoid, Fig. 3. A two step calibration of the sensors was implemented based on the following sensor models.

For the accelerometer:

$$\mathbf{a}_a = \mathbf{T}_a^{3\times 3}\left(\overline{\mathbf{a}}\| \left(\overline{g} + a(\overrightarrow{t})\right)\| + \overrightarrow{\mu}_a\right) + \mathbf{a}_0 \quad (5)$$

The affine transform $\mathbf{T}_a^{3\times 3}$ and offset $\mathbf{a}_0$ represent the accelerometer imperfections and are modeled as being time invariant. These include x,y and z axis misalignment within the sensor structure, gain variations of the sensor elements and other linear effects. Un-modeled accelerations $a(\overrightarrow{t})$ are expected to be of a higher frequency than the random walk caused by integrating noise in the angular rate gyro and would therefore be eliminated by the low pass effect of the complementary filter.

The magnetometer is modeled as follows:

$$\mathbf{m}_a = \mathrm{T}_m^{3\times 3}\overline{\mathbf{m}}(B_s) + \overrightarrow{\mu}_m + \mathbf{m}_0 \quad (6)$$

Where,

$$B_s = \|\overrightarrow{B}_0 + \overrightarrow{G_{\mathrm{ps}}(t)}s(x,y,z) + \overrightarrow{B_1(t)}|$$

The vector sum of the magnetic fields within the scanner reduces to the gradient z-axis. This is because the static magnetic field and time varying gradients are in the same direction. The radio frequency pulses, which are orthogonal to the z-axis, are negligible because of their small magnitude and high frequency. The magnetometer is slightly more vulnerable to distortion due to hard and soft iron effects. The matrix $\mathbf{T}_m^{3\times 3}$ models these effects along with other linear effects similar to the correction matrix used for the accelerometer. A once-off calibration sequence is therefore implemented similar to [17]. The individual sensor offsets and transformations are calculated by fitting a set of data points (preferably evenly distributed) to an ellipsoid using a constrained least squares algorithm Fig. 3. The calibration matrix then maps the fitted ellipsoid onto a unit sphere. The calibrated and scaled unit vectors form the accelerometer ā and magnetometer $\overline{\mathbf{m}}$ inputs to the observer (Fig. 2).

III. Materials and Methods

The following section describes the development of the orientation tracking hardware prototype (Figure 4). The computationally light-weight explicit complementary filter was implemented on a low power embedded device. A consumer grade inertial measurement unit (which contains the 3-axis accelerometer and angular rate gyro sensors) was used in the prototype design allowing for a low cost implementation. The magnetometer was however a more specialised part as the magnetic field strengths are far greater in the MRI scanner. Commercial parts are optimised for earth's field navigation. The use of the vector (cross-product) to generate the error function was much more computationally efficient because no formation of an unfiltered orientation quaternion was required. The MRI scanner passed both the RF noise and spike quality assurance tests supplied with the MRI scanner (3T, Skyra, Siemens, Erlangen, Germany) while the device was streaming orientation data from within the receive coil. The device artefacts penetrate approximately 10–15 mm into the image in the gradient echo pulse sequence implemented as can be seen in Figure 5 and therefore only has a significant effect on the signal strength in the skull/fat signal when mounted as shown in Figure 6.

A. Printed Circuit Board (PCB) design considerations

A four layer stack was used in the PCB layout. Signal traces on the top layer were routed to the inner layers as close to the integrated circuit footprints as possible. The remaining area was filled with a solid copper pour to shield the signals from the high power magnetic fields within the MRI scanner. The bottom layer was selected to be a solid pour with vias connecting the top and bottom layers around the periphery of the PCB in an attempt to make a Faraday cage around the signal traces. There was a trade off between the amount of copper used, which would interact with the gradient fields causing eddy currents which would vibrate the circuit as can be seen in Fig. 7, and the amount of radio frequency (RF) shielding. The 32-bit micro-controller is clocked at 32 MHz from an internal RC (resistor-capacitor) oscillator eliminating the need for an external quartz crystal. Quartz crystals are generally packaged in ferro-magnetic materials which can result in large image artefacts. This did however affect the maximum baud rate achievable over the serial link due to uncertainties in the oscillation frequency. A hot air solder levelling (HASL) finish was used for the footprints which is free from nickel (a major source of field interaction). Nonmagnetic capacitors (in small values) and resistors were used where possible. Power supply filtering was achieved using 10 μF tantalum capacitors in a plastic casing. Integrated circuits in certain quad flat no-leads (QFN) packages where free of nickel and could be used for the device's construction. A single cell, aluminium foil, lithium polymer battery pack with copper terminals was used to power the device (150 mAh) allowing 4 hours of continuous operation.

B. Plastic Optic Fibre Communication

The prototype uses a plastic fibre optic cable for unidirectional asynchronous serial communication with a laptop situated in the scanner control room (460800 bps). For improved performance data were transmitted in binary format of a fixed length. Each transmission contained 4 32-bit floating point values ($\hat{q}$), 9 16-bit integers ($\bar{a}$, $\overline{m}$, $\overline{\omega}$) followed

by a linefeed (0x0A) and carriage return (0x0D) for a total of 36 bytes. Data packets were transmitted at 300 packets/s to the laptop. A python thread would then poll the operating systems serial buffer ensuring no more than one packet was buffered at a time to improve latency. A real-time (60 fps) 3D representation of the orientation of the device is displayed on the laptop with data logging capabilities. The laptop is connected to the local scanner switch (1 Gigabit TCP/IP) allowing the scanner control computer to query the laptop for the latest orientation estimate. The latency for the laptop response to a scanner query was found to be less than 1 ms based on the scanner's μs clock (although this is dependent on the laptop's state).

IV. Results

The prototype device was tested to ensure safe and correct operation under scanning conditions. The alignment of the sensor and scanner co-ordinate frames was evaluated using high resolution 3D registrations. The potential for prospective motion correction (if combined with a translation measurement technique) was evaluated using controlled changes in orientation without translations. Finally, the application of the device to physiological motion measurement is presented.

A. MRI compatibility

To simulate a realistic positioning relative to the gradient iso-centre the device was mounted on a healthy subject's forehead (Fig. 6). All scans involving volunteers were conducted in accordance with protocols approved by the Faculty of Health Sciences Human Research Ethics Committee of the University of Cape Town. The data were collected in real time (300 Hz) during a 3D gradient echo pulse sequence. The angular rate gyro showed a slight bias (+ − 4 dps) dependent on the sensor's orientation relative to the static magnetic field, however the filter successfully tracks the biases with no noticeable effects on the output orientation. Interestingly these spurious biases are largely orthogonal to the static magnetic field and are therefore mitigated by the high precision magnetometer observation. Sufficient resolution of the subject's orientation is achieved to view the cardiac and respiration cycles. Referring to the data shown in the lowest plot of Fig. 7 it is evident that the device achieves the best performance about the axes tracked using the magnetometer. The z-axis shows the poorest performance due to the noise induced by field interactions even though the gradient interactions on the accelerometer dominate in the z-direction. This highlights the importance of the compensation block in the filter (Fig. 2).

B. Measuring Accuracy

To test the validity of the reference frame assumptions made, such as gravity and the static magnetic field being predefined in the imaging co-ordinate system due to the scanner's construction, orientation estimates were fed back to a 3D spoiled gradient echo pulse sequence (TR 10 ms, TE 8 ms, voxel size [P 0.7 mm, R 0.7 mm, S 2 mm]) without any scanner specific calibration. The orientation of the imaging pulse sequence was updated using orientation estimates from the sensor hardware. A pineapple phantom mounted on a mechanical 'wobbler' was used as the subject. The centre of rotation of the wobbler was aligned to the gradient iso-centre to minimise the amount of uncorrected translation. The

wobbler allows for controlled changes of the pineapple's orientation (+− 15 °) about a single axis at a time. The laptop logged the orientation estimate sent to the scanner control computer for each query. Each data point therefore corresponds to one TR of the imaging pulse sequence (first column of Fig. 8.)

For each movement of the pineapple, 3 images were obtained:

1. An image at the initial orientation.
2. An orientation 'corrected' image where the phantom was moved to a new orientation approximately 8 s into the acquisition. This was done early in the acquisition to ensure most of the data were captured in a frame defined by the device, giving a true representation of sensor frame errors.
3. An image at the final orientation.

To estimate the accuracy of the sensor defined co-ordinate frame the resulting 'orientation corrected' images (2) were compared to the result from a widely used 3D registration tool '*mri robust register*' [18]. Firstly, image (3) was registered to image (1). The registered image was then subtracted from image (1) and the absolute value of the difference at each voxel computed. The resulting difference image is plotted in the third column of Fig. 8 to illustrate the magnitude of registration errors arising from the rigid body fit. To reduce the impact of uncorrected translations on the difference image between the sensor corrected image (2) and original image (1), a translation only registration was implemented using the same software tool. Finally, the sensor corrected difference image was obtained by subtracting the (translation only) shifted image (2) from the initial image (1) (column 2 of Fig. 8). The orientation sensor showed comparable performance to the registration algorithm with peak differences occurring in similar locations. These changes are most likely as a result of inhomogeneities in the static field, and changes in RF receive sensitivity caused by motion. In all cases the registration algorithm converged to well within the recommended limits. The resulting transforms from the registrations were also compared to the change in orientation measured by the orientation sensing hardware (Table I). The magnitude of the angle measured by the hardware was consistently smaller than that of the registration algorithm (within a maximum difference of 0.8 degrees). The difference in axis of rotation is a result of misalignment between the measurement frames. The offset between the rotation axes was however very consistent over different angles for each of the controlled rotations and could be corrected by applying the measured deviations. This correction was not applied to the data presented here, so as to demonstrate the performance without scanner-specific calibration. However, this correction could be used as a method for real-time calibration when used alongside slower navigated methods. It was found that the reference frame errors were mostly in the positive × and negative z axes (both within 2 degrees, in our installation).

C. Evaluation of Dynamic Performance

The ability to correct for varying degrees of motion was evaluated with a series of dynamic scans. The pulse sequence parameters were changed to allow a shorter TR in this case (TR 7.5 ms, TE 3.76 ms, voxel size [P 0.7 mm, R 0.7 mm, S 4 mm]). The latency for each orientation update is determined by the pulse sequence repetition time (TR), the period

between data ready pulse on the sensor pin and data transmission of the orientation data ($t_{\text{filt}} \approx 900\ \mu s$), the laptop response delay ($t_{\text{delay}} < 1$ ms) and the frequency of the asynchronously transmitted data (300 Hz), therefore:

$$t_{\text{latency}} < \left(\frac{1}{300} + \text{TR} + t_{\text{filt}} + t_{\text{delay}}\right) = 12.7\text{ms}.$$

It is important to note that the dependence on pulse sequence repetition time is only due to practical limitations of updating the gradient co-ordinate frame once per readout and ensuring the gradient control buffer doesn't underflow. The quoted latency is an estimate of the maximum delay expected. Due to the undetermined nature of TC/IP, in some cases the delay (t_{delay}) would be longer than expected. In order to detect any unexpected delays the pulse sequence would log any instances in which the query for orientation wasn't serviced in time for the next sequence update, indicating a latency of greater than 2 TRs (15 ms). In the data presented (Figure 9) this only occurred a maximum of 2 times out of the 228 × 32 = 7296 lines acquired for that image. In each case the total acquisition time was 55 s. The results from least (top) to most (bottom) severe motion are presented in Figure 9.

D. In Vivo Involuntary Changes in Orientation

Raw data in all 3 axes showed a strong correspondence to a 4 channel electro-cardiogram (ECG) signal obtained (Fig. 10) while a subject lay motionless within the MRI scanner. High and Bandpass filtering the signal with a zero-phase digital filter allowed for the separation of 'cardiac' and 'respiration' signals respectively. The nodding motion detected here could be due to skin motion pulsations from small sub-cutaneous blood vessels or blood pressure fluctuations in the carotid arteries. Aortic valve regurgitation can result in a visible head motion such as *Corrigan* and *de Mussets* signs. The nodding pulsations detected could be due to a similar phenomenon at a much smaller scale in the healthy subjects scanned.

V. Discussion

Field interactions with the sensing device are the major contributor to noise in the orientation estimates and image artefacts (in close proximity to the device). The sensor PCB and battery size therefore play a significant role in the performance of the orientation estimates. The initial prototype could be improved by reducing the overall size of the hardware. The high precision required for prospective motion correction is vulnerable to non-rigid sensor motion relative to the imaged object. The use of a plastic fibre optic cable was not ideal for sensor mounting where the stiff cable could mechanically induce spurious changes in the sensor position. This was however an experimental layout of the hardware which showed very good MRI compatibility where a standoff distance of only 10 mm was sufficient to eliminate most visible image artefacts (Figure 5) in the gradient echo sequence implemented. Alternative communication techniques could include wireless electromagnetic approaches which are well outside the operating frequency of the MRI scanner or wireless optical techniques. It is important for the communication protocol to achieve a low latency and high frequency as we noticed angular rates of change as large as 20 dps during 'normal'

subject motion which would correlate to 0.15 degrees per TR of the gradient echo sequence implemented in this paper. In order to achieve sub voxel resolution motion correction in structural scans without rejecting any data, one would require exceptionally high temporal resolution sequence updates. The data streamed from the device includes angular rate and acceleration which could be used to predict the future position/orientation of the subject for improved performance.

There is a strong correlation between the change in the subject's head orientation and the translation of the subject in the field of view. The majority of the subject motion occurs whilst their head remains in contact with the cushion within the MR receiver coil and can be estimated as rolling motion. Cardiac and respiration contribute to pulsatile motion in healthy subjects on the order of 0.14 degrees peak to peak. When imaging the frontal pole that lies approximately 150 mm from the subject's contact point these signals would correspond to voxel blurring over an arc length of 0.4 mm for involuntary motion, highlighting the importance of precise orientation estimation. The high temporal resolution estimates would therefore be well suited for combining with slower navigator based approaches where the orientation estimates, patient motion model and slower navigator data could be combined for a complete prospective motion correction solution.

VI. Conclusion

The method presented for orientation measurement can be set up in an untouched scanner in a few minutes with no alterations to the scanner hardware. The technique uses mostly consumer grade integrated circuit components and as a result implementation costs were low, less than US$ 1 000 for three completed prototypes as presented here. The method can correct for large changes in orientation at a high temporal resolution (each line of k-space) with minimal impact on the imaging pulse sequence. The method has shown the potential to detect small periodic changes in orientation such as the subject's breathing and pulse which could be valuable for gating of imaging pulse sequences which are susceptible to blood flow or respiration. The calibration free implementation presented has the potential to make prospective motion correction using external hardware more relevant to a clinical environment, where measuring orientation has restricted marker placement and size or is reliant on pulse sequence modifications. The new method (VectOrient) implemented in this work was capable of correcting very rapid motion, achieving a latency of less than 12.7 ms to an accuracy of within 0.8 degrees over +−15 degree rotations. The precision of the angular rate sensor and magnetometer allows the quantification of subject pulse. Most of the latency in the current implementation comes from communication and the sequence update framework, where processing of the sensor signal contributes to less than a millisecond of the total delay. VectOrient would therefore have the potential to ensure robust encoding of the magnitude of the raw MR signal even during high angular rates of change (> 20 dps) if low latency access to the gradient amplifier rotation matrix was made available.

Acknowledgments

This work was supported in part by the National Institutes of Health under grants R01HD071664 R21MH096559, the NRF/DST through the South African Research Chairs Initiative and the University of Cape Town through the Sir Robert Kotze Fellowship and RCIPS Explorer fund EX15-009.

References

1. Maclaren J, Armstrong BSR, Barrows RT, Danishad KA, Ernst T, Foster CL, Gumus K, Herbst M, Kadashevich IY, Kusik TP, Li Q, Lovell-smith C, Prieto T, Schulze P, Speck O, Stucht D, Zaitsev M. Measurement and Correction of Microscopic Head Motion during Magnetic Resonance Imaging of the Brain. PLoS ONE. 2012; 7(11):3–11.
2. Soellinger M, Rutz AK, Kozerke S, Boesiger P. 3D cine displacement-encoded MRI of pulsatile brain motion. Magnetic Resonance in Medicine. 2009; 61(1):153–162. [PubMed: 19097224]
3. Hess AT, Tisdall MD, Andronesi OC, Meintjes EM, van der Kouwe AJW. Real-time motion and B0 corrected single voxel spectroscopy using volumetric navigators. Magnetic Resonance in Medicine. Aug; 2011 66(2):314–23. [PubMed: 21381101]
4. White N, Roddey C, Shankaranarayanan A, Han E, Rettmann D, Kuperman J, Dale A. Prospective Real-Time Correction for Arbitrary Head Motion Correction in MRI using Image-based Tracking. Magnetic Resonance in Medicine. 2010; 63(1):91–105. [PubMed: 20027635]
5. van der Kouwe AJW, Benner T, Dale AM. Real-Time Rigid Body Motion Correction and Shimming Using Cloverleaf Navigators. Magnetic Resonance in Medicine. 2006; 1019–1032(56):1019–1032.
6. Kober T, Marques JP, Gruetter R, Krueger G. Head motion detection using FID navigators. Magnetic Resonance in Medicine. Jul; 2011 66(1):135–43. [Online]. Available: http://www.ncbi.nlm.nih.gov/pubmed/21337424. [PubMed: 21337424]
7. Ooi, MB., Aksoy, M., Maclaren, J., Watkins, RD., Bammer, R. Prospective motion correction using inductively coupled wireless RF coils. Magnetic Resonance in Medicine. Jun. 2013 [Online]. Available: http://www.ncbi.nlm.nih.gov/pubmed/23813444
8. Nevo, E. Method and apparatus to estimate location and orientation of objects during magnetic resonance imaging. Feb. 2003 [Online]. Available: http://www.google.com/patents/US6516213
9. Haeberlin M, Kasper L, Barmet C, Brunner DO, Dietrich BE, Gross S, Wilm BJ, Kozerke S, Pruessmann KP. Real-Time Motion Correction Using Gradient Tones and Head-Mounted NMR Field Probes. Magnetic Resonance in Medicine. 2015; 660(74):647–660.
10. Zaitsev M, Dold C, Sakas G, Hennig J, Speck O. Magnetic resonance imaging of freely moving objects: prospective real-time motion correction using an external optical motion tracking system. NeuroImage. Jul; 2006 31(3):1038–50. [Online]. Available: http://www.ncbi.nlm.nih.gov/pubmed/16600642. [PubMed: 16600642]
11. Zahneisen B, Lovell-Smith C, Herbst M, Zaitsev M, Speck O, Armstrong B, Ernst T. Fast noniterative calibration of an external motion tracking device. Magnetic Resonance in Medicine. Apr; 2014 71(4):1489–500. [Online]. Available: http://www.ncbi.nlm.nih.gov/pubmed/23788117. [PubMed: 23788117]
12. Schulz J, Siegert T, Reimer E, Labadie C, Maclaren J, Herbst M, Zaitsev M, Turner R. An embedded optical tracking system for motion-corrected magnetic resonance imaging at 7T. Magnetic Resonance Materials in Physics, Biology and Medicine. 2012; 25(6):443–453.
13. Armstrong B, Verron T, Heppe L, Reynolds J, Schmidt K. RGR-3D: Simple, Cheap detection of 6-DOF Pose for Tele-Operation, and Robot Programming and Calibration. Proceedings 2002 IEEE International Conference on Robotics and Automation (Cat No.02CH37292). May.2002 3
14. Mahony R, Hamel T, Pflimlin J-M. Nonlinear Complementary Filters on the Special Orthogonal Group. IEEE Transactions on Automatic Control. Jun; 2008 53(5):1203–1218. [Online]. Available: http://ieeexplore.ieee.org/lpdocs/epic03/wrapper.htm?arnumber=4608934.
15. Madgwick SOH, Harrison AJL, Vaidyanathan R. Estimation of IMU and MARG orientation using a gradient descent algorithm. IEEE International Conference on Rehabilitation Robotics. 2011
16. Markley F. Attitude Determination Using Vector Observations and the Singular Value Decomposition. Journal of the Astronautical Sciences. 1988; 36(3):245–258.
17. Liu Y, Li X, Zhang X, Feng Y. Novel Calibration Algorithm for a Three-Axis Strapdown Magnetometer. Sensors. 2014; 14(5):8485–8504. [Online]. Available: http://www.mdpi.com/1424-8220/14/5/8485/. [PubMed: 24831110]
18. Reuter M, Rosas HD, Fischl B. Highly accurate inverse consistent registration: A robust approach. NeuroImage. 2010; 53(4):1181–1196. [PubMed: 20637289]

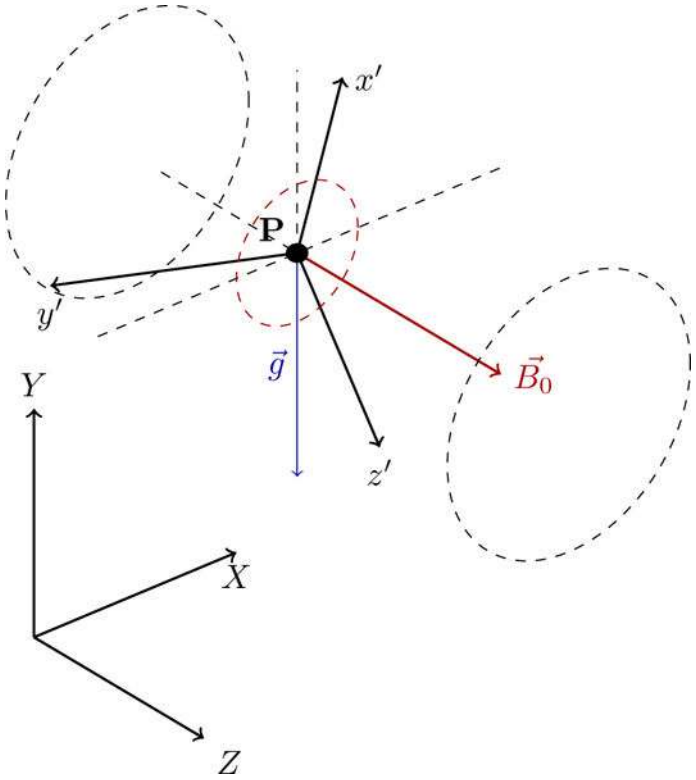

Fig. 1.

Sensor frame ($x'y'z'$) relative to the scanner co-ordinate frame (XYZ), the large dotted circles represent the MRI scanner bore. The ground lies parallel to the XZ plane.

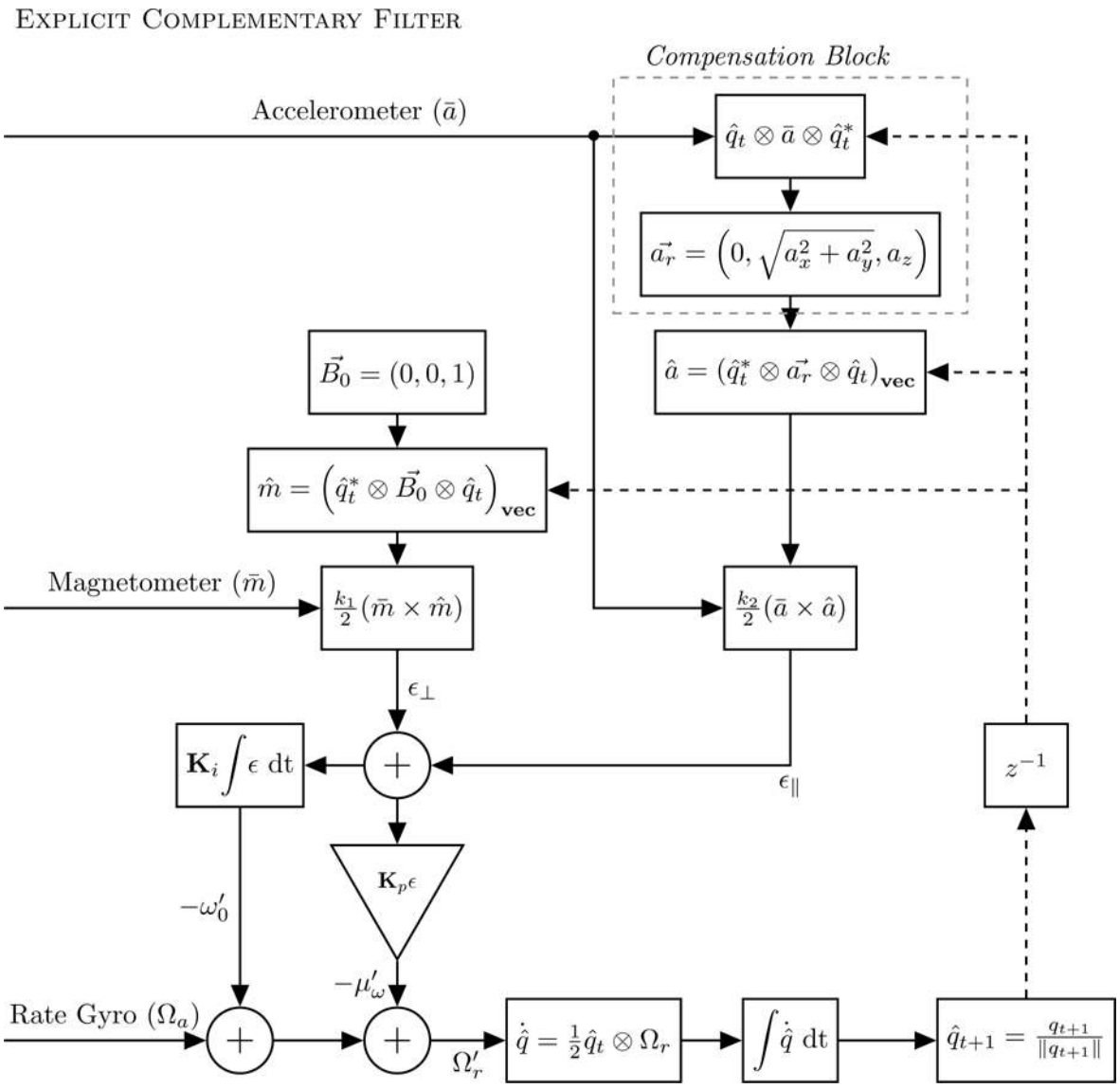

Fig. 2.

Explicit (vector based) complementary filter with angular rate gyro bias compensation. $\hat{q}$ symbol designates a unit quaternion and ⊗ represents quaternion multiplication. All vectors are unit in magnitude and the × symbol represents the vector cross product. The output of the filter $\hat{q}_{t+1}$represents the scanner co-ordinate system (*scs*) with respect to the device co-ordinate system (*dcs*). Primes denote estimates of the gyro bias $(\omega_0^{'})$ and imperfections $(\mu_\omega^{'})$.

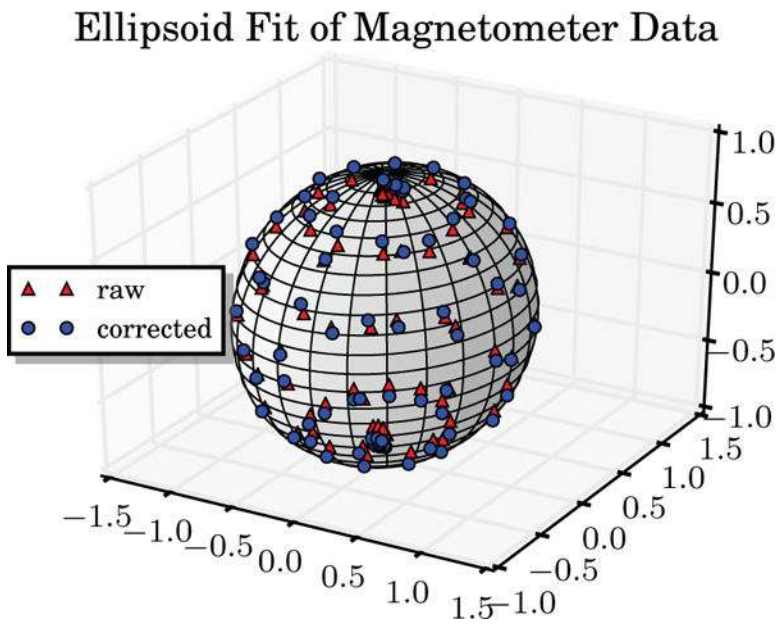

Fig. 3.

Circles are the calibrated data fit to a unit sphere. Notice the scaling of the uncalibrated (raw) triangles in the vertical axis. This could be expected as the z-axis sensing element is structurally different to the ones lying on the plane of the integrated circuit.

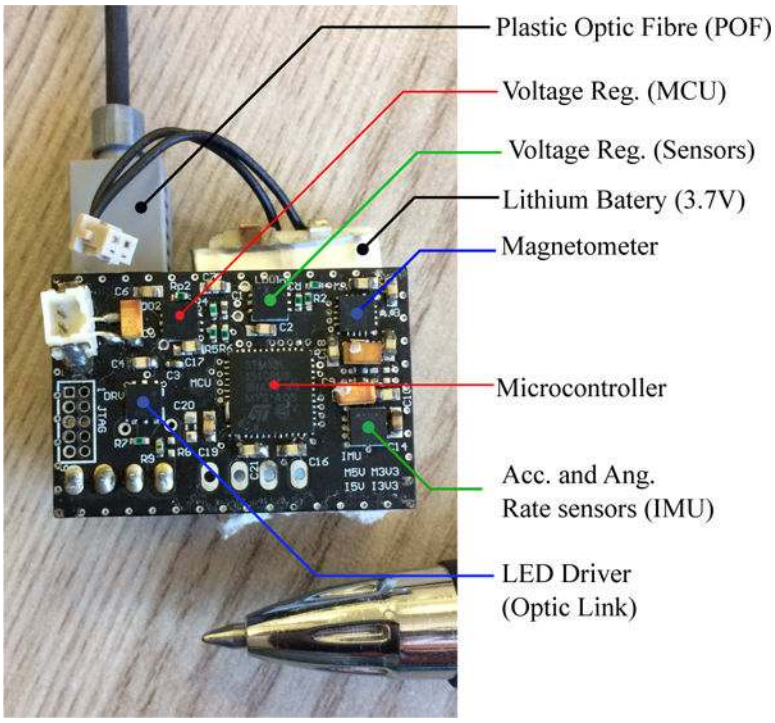

Fig. 4.

Prototype hardware. The larger IC in the centre is the Micro-controller. Underneath left is the optical transmitter. Right of the MCU are the sensors.

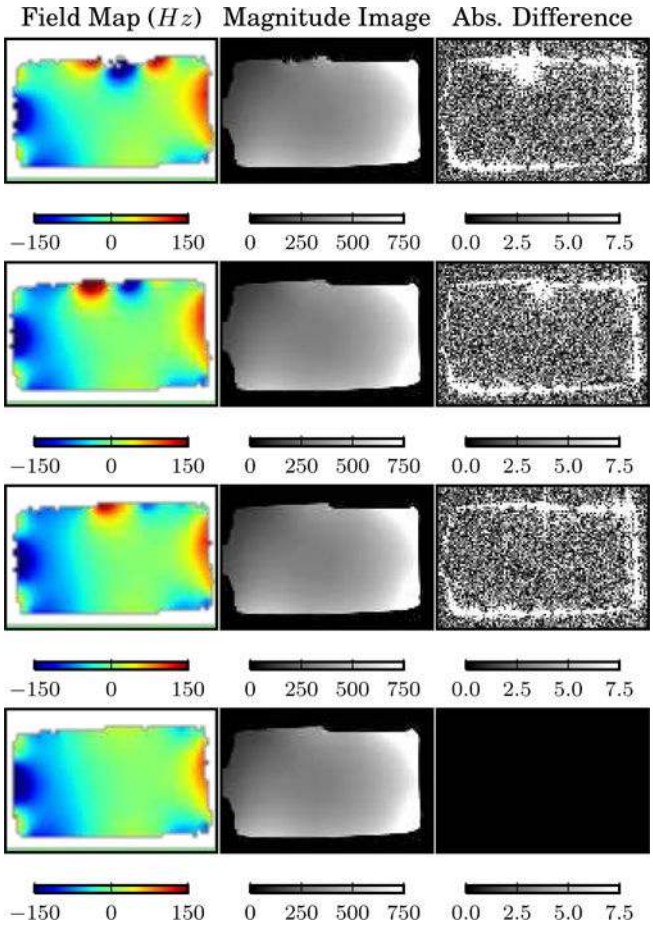

Fig. 5.

From top to bottom rows the device was placed directly against the cylindrical phantom; 10 mm normal to the top surface; 20 mm normal to the top surface; and finally imaged without the device present. The gradient echo images (TR 10 ms, TE 5 ms, voxel size [P 0.7 mm, R 0.7 mm, S 1 mm]) were obtained in a different series of scans with the same sensor offsets relative to the phantom surface. All difference images are computed relative to the magnitude image acquired without a device.

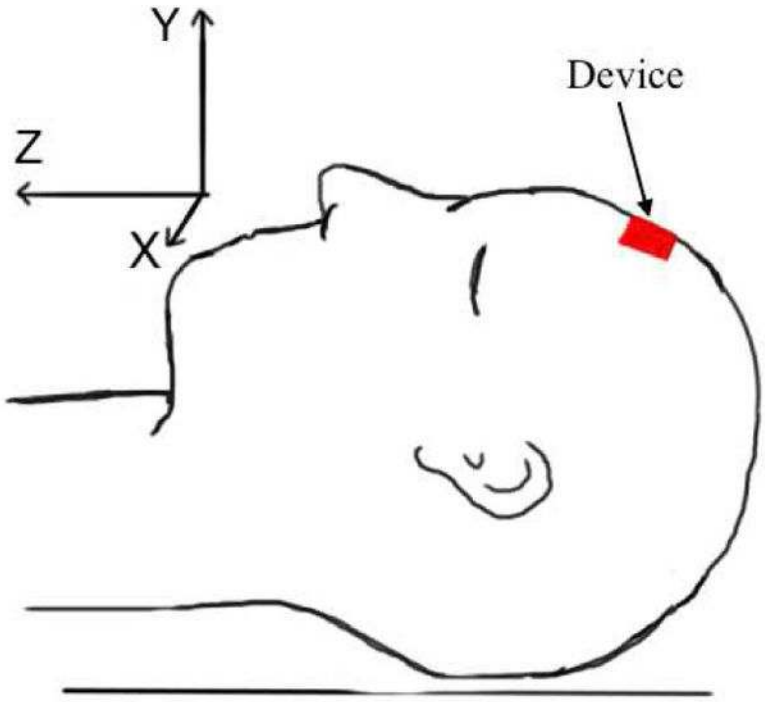

Fig. 6.

The sensor was mounted on the patient's forehead using double sided tape for the human physiological data acquired. Due to the small size of the device and small magnitude of the gradient torques, no abnormal heating (typically ≈ 0.2°C) could be detected using the embedded (Magnetometer and IMU) temperature sensors. In some cases the ground plane temperature decreased during scanner operation.

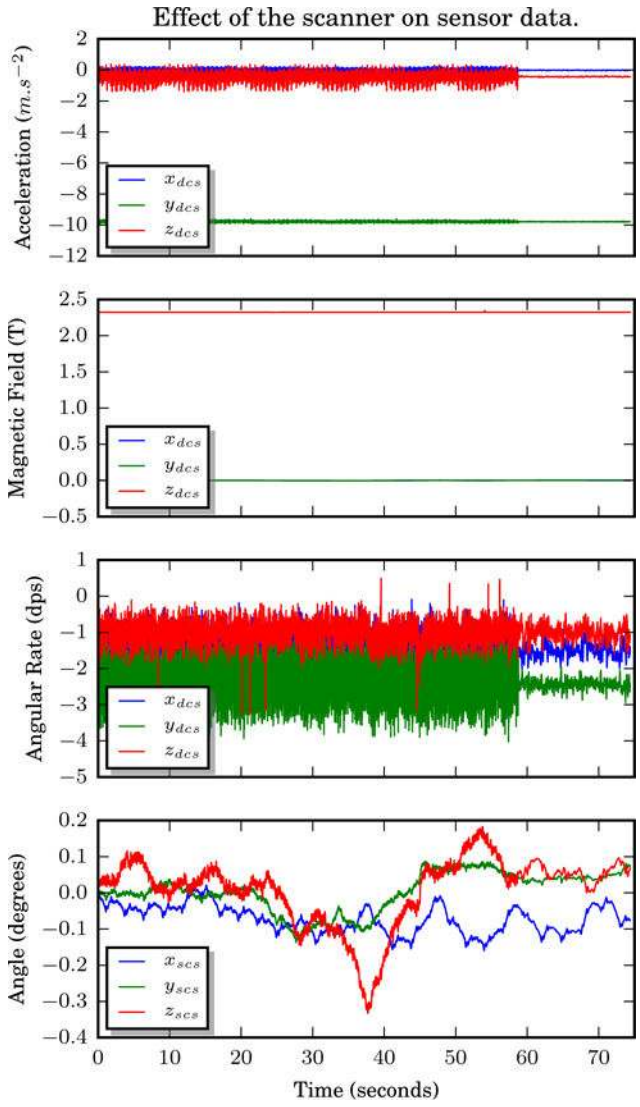

Fig. 7.

Effect of gradient activity on accelerometer and angular rate measurements. Data were logged during an MR acquisition (first 58s, gradient echo pulse sequence) and continued after the pulse sequence had ended (roughly last 15s of the plot). The relatively high temporal resolution signal, present while the scanner is active, is periodic and well correlated with the repitition time (TR; 10 ms) of the imaging pulse sequence. This is most likely caused by eddy current interactions with the static magnetic field causing vibrations of the scanner bed and/or PCB. Secondary effects could include diodes in the measurement circuit rectifying induced currents or field interactions with the micro-electromechanical elements. Data displayed was recorded while attached to a subject, hence the visible involuntary changes in orientation.

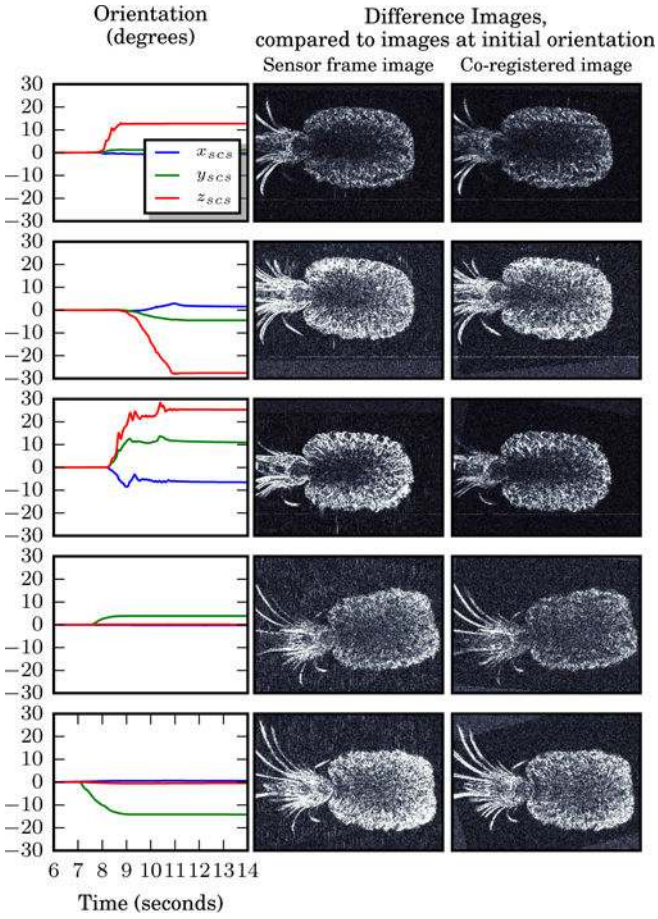

Fig. 8.

Comparison of the sensor frame to a high resolution registration. All images are scaled 0–25% relative to the first uncorrupted image at the initial positions to more clearly show subtle differences. The first column shows the change in orientation applied to the pineapple for each of the 5 tests. The motion of tests 0–2 were achieved by hand, hence the more shaky changes.

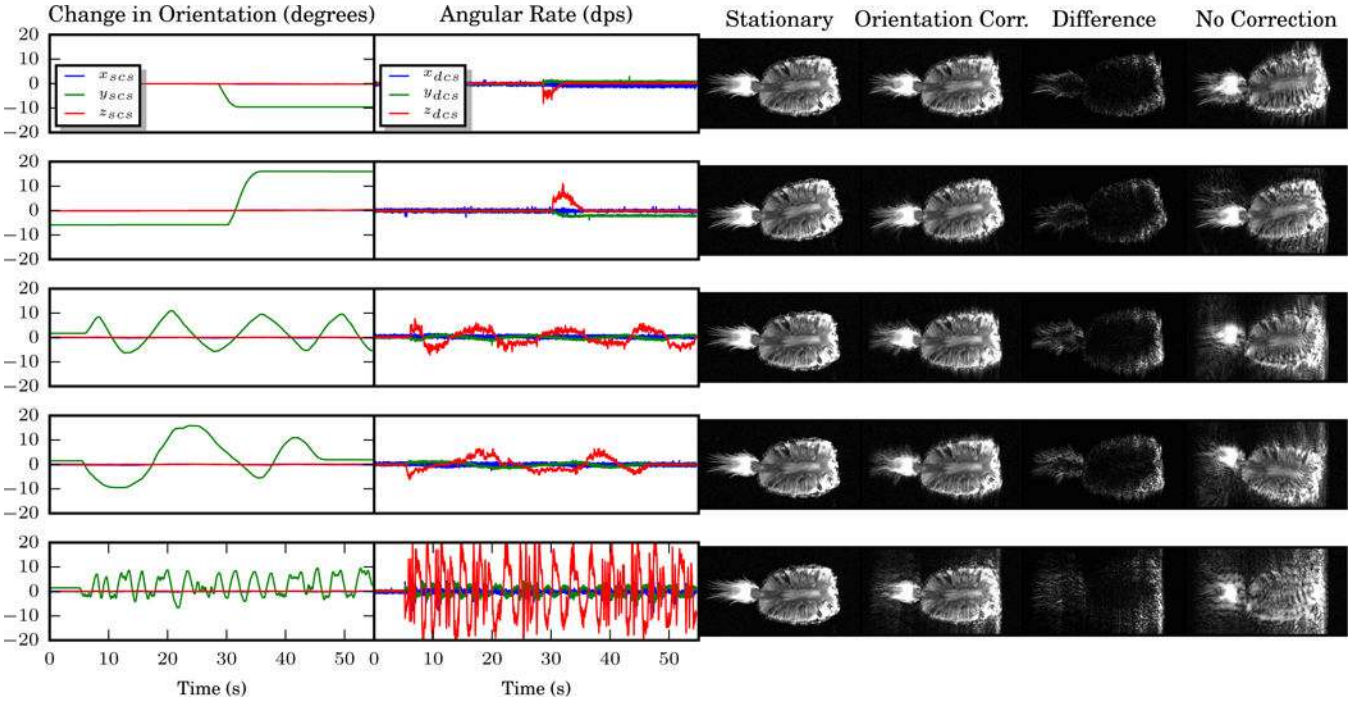

Fig. 9.

Evaluation of dynamic performance for the potential application of prospective motion correction. The change in orientation is plotted relative to the very first scan in the series presented (top, left). The angular rate gives an indication of the severity of the motion. Difference images present absolute values from a voxel-wise subtraction of the stationary and orientation corrected images. In each case the 'No correction' image was collected under replicated motion, similar in amplitude and timing without orientation updates applied. In the final row the prospective orientation correction begins to fail as more blurring artefacts are present. This row does however represent an exceptional case with 26 changes of ≈10° and 40 changes of 3°–5° over a 50 second scan.

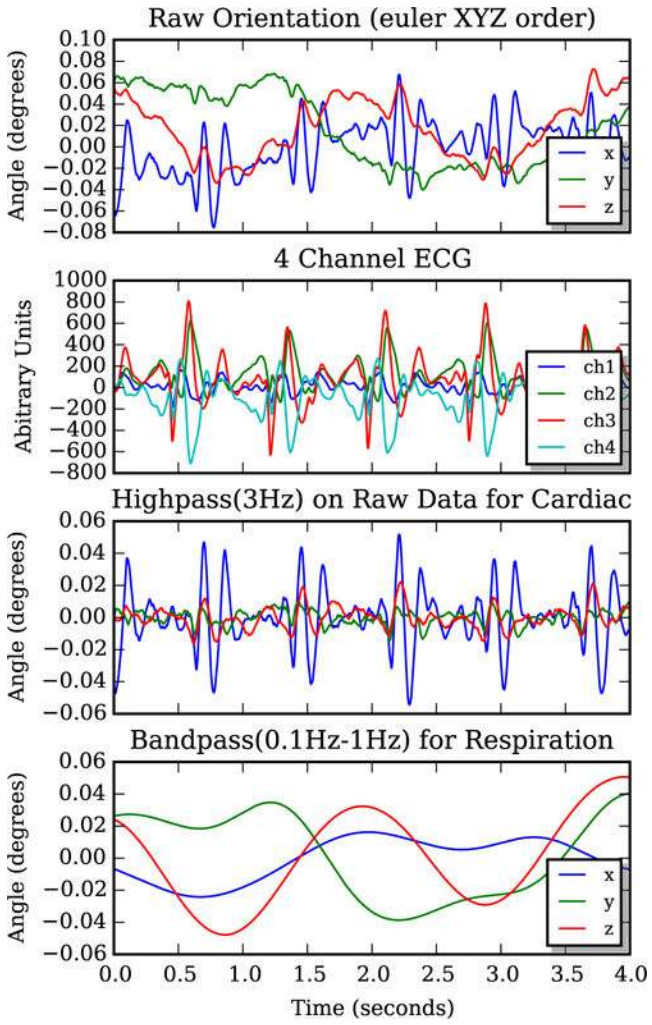

Fig. 10.

The sensor array is able to pick up a unique patient signature which correlates well with their pulse and respiration. The data presented above was acquired while the MRI scanner was inactive with the marker attached to the subject's forehead. A 3 Hz high-pass filter was selected to reduce base line drift from respiratory motion in the plot of orientation data representing involuntary cardiac motion.

TABLE I

Changes in Orientation in Scanner Frame

Dataset	Registration (deg.[axis])	Sensor (deg.[axis])
Test 0	13.56(−0.064,0.110,−0.992)	13.31(−0.062,0.089,−0.994)
Test 1	28.59(0.006,−0.193,0.981)	28.23(0.002,−0.169,0.986)
Test 2	28.46(−0.304,0.359,−0.883)	27.62(−0.315,0.322,−0.893)
Test 3	4.08(−0.018,1.000,0.012)	3.85(−0.051,0.998,−0.022)
Test 4	14.96(0.004,−1.000,−0.011)	14.18(0.033,−0.999,0.032)